Verdin, A., Malherbe, C., Sloan-Dennison, S., Faulds, K., Graham, D., & Eppe, G. (2024). Thiol-polyethylene glycol-folic acid (HS-PEG-FA) induced aggregation of Au@Ag nanoparticles: a SERS and extinction UV–Vis spectroscopy combined study. *Spectrochimica Acta - Part A: Molecular and Biomolecular Spectroscopy*, *322*, Article 124848. Advance online publication. https://doi.org/10.1016/j.saa.2024.124848

Thiol-polyethylene glycol-folic acid (HS-PEG-FA) induced aggregation of Au@Ag nanoparticles: a SERS and Extinction UV-Vis Spectroscopy combined study.

Alexandre Verdin[1], Cedric Malherbe[1], Sian Sloan-Dennison[2], Karen Faulds[2], Duncan Graham[2] and Gauthier Eppe[1].

[1]*Mass Spectrometry Laboratory, MolSys Research Unit, University of Liège, Belgium.*

[2]*Department of Pure and Applied Chemistry, Technology and Innovation Centre, University of Strathclyde, 99 George Street, Glasgow G1 1RD, UK.*

Abstract

Plasmonic colloidal nanoparticles (NPs) functionalised with polymers are widely employed in diverse applications, offering advantages demonstrated over non-functionalised NPs such as enhanced colloidal stability or increased biocompatibility. However, functionalisation with polymers does not always increase the stability of the colloidal system. This work explores the intricate relationship between the functionalisation of plasmonic core@shell Au@Ag nanoparticles (NPs) with thiol-polyethylene glycol-folic acid (HS-PEG-FA) polymer chains and the resulting stability and spectral characteristics of Surface-Enhanced Raman Scattering (SERS) nanotags based on these NPs. We demonstrate that varying levels of HS-PEG-FA grafting influence nanotag stability, with a low level of grafting causing aggregation and subsequently affecting the spectral signature of Raman-reporter molecules attached to the surface of the NP. Electrostatic destabilisation is identified as the primary mechanism driving aggregation, impacting the SERS spectrum of Malachite Green isothiocyanate (MGITC) whose spectral shape is different between the aggregated and non-aggregated NPs. The findings provide valuable insights into NPs stability under different conditions, offering essential considerations for the design and optimisation of SERS nanotags in bio-analytical applications, particularly those involving data processing based on spectral shape, such as in multiplex approaches where experimental spectra are decomposed with several reference components.

Verdin, A., Malherbe, C., Sloan-Dennison, S., Faulds, K., Graham, D., & Eppe, G. (2024). Thiol-polyethylene glycol-folic acid (HS-PEG-FA) induced aggregation of Au@Ag nanoparticles: a SERS and extinction UV–Vis spectroscopy combined study. *Spectrochimica Acta - Part A: Molecular and Biomolecular Spectroscopy*, *322*, Article 124848. Advance online publication. https://doi.org/10.1016/j.saa.2024.124848

1. Introduction

Plasmonic nanoparticles (NPs) have recently found applications in many fields owing to their unique optical properties [1]–[4]. Moreover, functionalisation of their surface by polymers has been widely applied to finely tune the physicochemical characteristics of NPs [5]–[7]. Adding polymers to the surface of NPs provides several advantages, such as increased colloidal stability, increased biocompatibility, reduction of protein corona formation and resistance to enzymatic degradation, or ease of further functionalisation [5],[7]. Polymers can also bring additional properties to the NPs, such as the ability to respond to heat [8], redox potential [9] or pH [10], [11] variations, allowing control of the supramolecular assembly of NPs [12], [13] or the release of drugs from nanocarriers [14]. One particular area of interest for the use of plasmonic NPs is in Surface-Enhanced Raman Scattering (SERS) for the highly sensitive sensing of molecules adsorbed to the NPs [1], [15], [16]. In SERS, the plasmonic nature of the NPs is exploited to increase the electric field felt by molecules close to the surface of the NPs when monochromatic light is used to excite the sample, giving rise to a huge enhancement in signal intensity compared to classical Raman scattering [15]. The high sensitivity provided by the SERS effect can also be used to design spectroscopic tags, achieved by labelling the surface of the NPs with molecules with known Raman spectrum, denoted as Raman-reporter molecules [17]. These SERS nanotags have found plenty of applications in biological sensing and are widely regarded as a promising alternative to other kinds of optical labels, such as fluorescent molecules [18]–[21]. The surface of SERS nanotags is usually protected with a coating to guarantee their stability in biological media with high ionic strength, to prevent surface adsorption of endogenous molecules and to reduce non-specific interactions. A wide diversity of coating (either inorganic or organic) can be found, but polymers remain a popular choice owing to their aforementioned advantageous characteristics. More particularly, polyethylene glycol (PEG) is the most common option because of its high biocompatibility and its strong ability to reduce protein corona formation and non-specific interactions [22]–[24]. PEG chains can be easily modified with a thiol function on the chain end to allow nearly covalent grafting on the surface of gold (Au) or silver (Ag) NPs [25], [26], which are the most popular plasmonic NPs used for SERS applications. Thanks to the anchoring point provided by the thiol function and to the hydrophilic nature of PEG, HS-PEG chains form an extended, compact and highly hydrated corona around the NPs, strongly shielding the surface of the NPs from the medium by excluded volume effects [27]. Chain tail flexibility is also an important parameter to reduce adsorption of proteins from the medium; and flexibility increases with the polymer chain length [28]. During the formation of SERS nanotags, thiolated PEG chains are grafted along the Raman-reporter molecules on the surface of plasmonic NPs. Raman-reporter molecules allow the spectroscopic labelling of the NPs, while the PEG coating provides high colloidal stability and reduces non-specific interactions once the nanotags are introduced in complex media.

Verdin, A., Malherbe, C., Sloan-Dennison, S., Faulds, K., Graham, D., & Eppe, G. (2024). Thiol-polyethylene glycol-folic acid (HS-PEG-FA) induced aggregation of Au@Ag nanoparticles: a SERS and extinction UV–Vis spectroscopy combined study. *Spectrochimica Acta - Part A: Molecular and Biomolecular Spectroscopy*, *322*, Article 124848. Advance online publication. https://doi.org/10.1016/j.saa.2024.124848

Furthermore, chemical functionalities at the other end of HS-PEG chains can be introduced and enable further coupling of biomolecules for targeting purpose. In our previous work, we used HS-PEG chains terminated with folic acid (FA) (denoted HS-PEG-FA) [29]. FA is widely used in the context of cancer cell imaging and targeting because of the well-established overexpression of folate receptors (mostly Folate Receptor α) on the membrane of cancer cells [30]. FA therefore allows nanotags to be directed to the cancer cells, enabling their detection with a high specificity compared to healthy cells [31]. Other groups have also functionalised SERS nanotags with PEG-FA chains to detect cancer cells, highlighting the high interest of using such coatings in bio-analytical applications [32]–[35].

However, in our recent experimental investigations, we observed that the level of HS-PEG-FA grafting (i.e. the number of chains per NP) can influence the stability of the nanotags, and subsequently also influence the spectrum of the Raman-reporter molecules used for spectroscopic labelling. The origin of these effects is not well understood and, in this work, we try to bring insights into the destabilisation mechanism induced by HS-PEG-FA polymeric chains on core@shell Au@Ag NPs. We report that the HS-PEG-FA chains can induce aggregation of the Au@Ag NPs at certain concentrations, and that the spectral signature of Raman-reporter molecules is strongly influenced by the aggregation process. We investigated the origin of the PEG-induced aggregation by various techniques and demonstrated that electrostatic destabilisation was the main driving force. These findings emphasize the necessity of properly optimising the PEG grafting level on Au@Ag NPs to ensure colloidal stability. We also investigated the effect of aggregation on the SERS spectrum of Malachite Green isothiocyanate (MGITC, Raman-reporter molecule) and demonstrated that MGITC molecules trapped in NP aggregates exhibit a different spectral shape than MGITC molecules on non-aggregated NPs, probably due to increased inter-molecular interactions inside the aggregates. This is important as aggregates produce much brighter SERS signals than well dispersed NPs, contributing strongly to the overall spectral shape even when aggregation is low. Our study provides efficient tools to rationalise the stability of NPs in various conditions, and emphasizes that even a low degree of aggregation cannot be neglected when studying the spectral shape of Raman-reporter molecules. This could be particularly important in the context of SERS nanotags for approaches where experimental SERS spectra are fitted with the reference spectrum of the reporter molecule [29], [36], [37], since changes in band ratio caused by aggregation could alter the results of such analysis.

Verdin, A., Malherbe, C., Sloan-Dennison, S., Faulds, K., Graham, D., & Eppe, G. (2024). Thiol-polyethylene glycol-folic acid (HS-PEG-FA) induced aggregation of Au@Ag nanoparticles: a SERS and extinction UV–Vis spectroscopy combined study. *Spectrochimica Acta - Part A: Molecular and Biomolecular Spectroscopy*, *322*, Article 124848. Advance online publication. https://doi.org/10.1016/j.saa.2024.124848

2. Material and methods

Gold NPs (diameter = 30 nm) used as core for the Au@Ag NPs synthesis were purchased from nanoQoloids (Belgium) at a concentration of $2.5x10^{11}$ NP/mL (optical density = 4 at 529 nm). MGITC was purchased from ThermoFisher and thiol-PEG-folic acid (HS-PEG-FA, 5000 g/mol) was purchased from Abbexa.

25 µL of freshly prepared MGITC 10^{-5} M was incubated with 250 µL of Au@Ag NPs (diameter of 45 nm, $2.5x10^{11}$ NP/mL). Details for the synthesis of the core@shell Au@Ag NPs can be found elsewhere [38]. Description of the optical properties and SERS performances of the Au@Ag NPs and of the core gold NPs have been deeply investigated in our previous work [38]. After incubation, NPs were centrifuged at 3200 RCF during 15 min, rinsed and finally resuspended in 0.05 M HEPES buffer at pH = 6.6. Finally, MGITC-labelled Au@Ag NPs were incubated with various amounts of HS-PEG-FA at stock concentration of $5x10^{-5}$ M to produce solutions with [HS-PEG-FA] ranging from 10^{-7} to $2x10^{-5}$ M. For studying the isolated aggregates, MGITC-labelled Au@Ag NPs were incubated with HS-PEG-FA at $4x10^{-7}$ M at pH = 6.6 for 30 min and then centrifuged at 900 RCF for 10 min. In these conditions, only a very low number of NPs was deposited at the bottom of the Eppendorf, corresponding to the heavier fraction of the solution and therefore mainly composed of the aggregates. The supernatant was carefully removed and aggregates were dispersed in water for further analysis.

SERS spectra of the different solutions were measured through glass vials with the solution under magnetic stirring (300 RPM). Raman analysis were performed with a Horiba Jobin Yvon Labram 300 spectrometer coupled to an Olympus BX40 microscope. Spectra were recorded under 532 nm irradiation through a 5x microscope objective, with an approximate power at the sample of 7 mW and 20x1 s of signal acquisition. Grating of 1800/mm was used for all measurements. SERS kinetic measurements were performed by measuring the SERS spectrum with a single acquisition of 1 s every 3 s of the experiment with the same parameters as above. Measured SERS spectra were zoomed in the spectral range of interest (either 1100-1700 cm^{-1} or 700-1700 cm^{-1}) and baseline-corrected using a 5^{th} order polynomial fit (Savitsky-Golay). Spectra were then normalised to the main band of MGITC at 1615 cm^{-1}.

UV-Visible (UV-Vis) extinction spectra of the samples were measured through PMMA cuvettes with 1 cm of optical path. Samples were diluted by HEPES buffer (pH = 6.6) before

Verdin, A., Malherbe, C., Sloan-Dennison, S., Faulds, K., Graham, D., & Eppe, G. (2024). Thiol-polyethylene glycol-folic acid (HS-PEG-FA) induced aggregation of Au@Ag nanoparticles: a SERS and extinction UV–Vis spectroscopy combined study. *Spectrochimica Acta - Part A: Molecular and Biomolecular Spectroscopy*, *322*, Article 124848. Advance online publication. https://doi.org/10.1016/j.saa.2024.124848

measurement on a Perkin Elmer Lambda 25 spectrometer operating in the 800-330 nm range of wavelength. UV-Vis kinetic measurements were performed by measuring a complete spectrum every 2 minutes. A spectrum acquisition took approximately 30 s. UV-Vis extinction spectra were normalised to the extinction of the maximum with no further processing. Zeta potential and Dynamic Light Scattering (DLS) measurements were performed on a Malvern Nanosizer Nano ZS and the NPs concentration was of $2.5x10^{10}$ NPs/mL. Negatively-charged 40 nm polystyrene beads were measured as reference material before running the samples.

3. Results and discussion

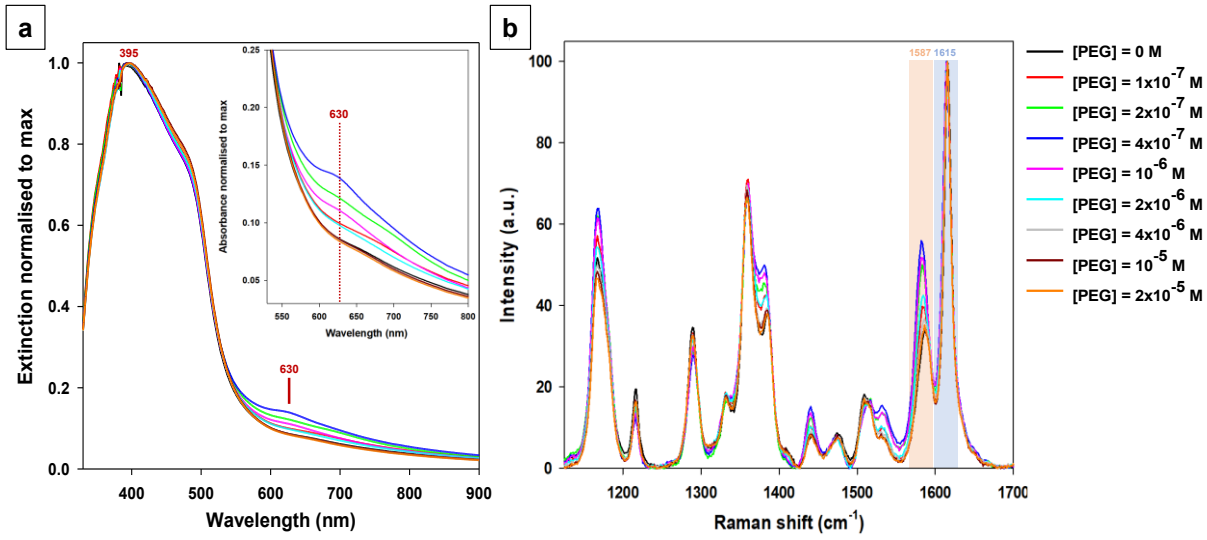

Figure 1. (a) UV-Vis extinction spectra of MGITC-functionalised Au@Ag NPs after 30 min of incubation in HEPES buffer at pH = 6.6 with various concentration of HS-PEG-FA. Insert shows a zoom on the wavelength range from 530 to 800 nm. Wavelengths at which the extinction values were extracted to evaluate the extinction ratio are indicated. (b) Corresponding SERS spectra of MGITC-functionalised Au@Ag NPs with increasing concentration of HS-PEG-FA obtained under 532 nm irradiation with a laser power of 7 mW at the sample and 20 acquisitions of 1 s. The bands used for the aggregation analysis are highlighted in orange (1587 cm^{-1}) and blue (1615 cm^{-1}).

3.1. UV-Visible extinction spectroscopy study

We investigated functionalising a large range of HS-PEG-FA concentrations to Au@Ag NPs and we characterised the colloidal stability by UV-Visible extinction spectroscopy and with SERS. UV-Vis extinction spectra show the extinction band attributed to the Localised Surface Plasmon Resonance (LSPR) at around 395 nm, which is characteristic of well dispersed Au@Ag NPs (Figure 1a) [29], [38]. For some PEG concentrations in the investigated range (10^{-7} to $2x10^{-5}$ M), an increase of the extinction at higher wavelengths (between 550 and 800 nm) is observed after 30 min of incubation, suggesting slight aggregation of the NPs (Figure 1a). Note that the highest degree of aggregation induced by PEG in these experiments was small compared to salt-induced aggregation, and PEG-aggregated NPs remained stable for a long time period (several days). For some other PEG concentrations in the same range, the UV-

Verdin, A., Malherbe, C., Sloan-Dennison, S., Faulds, K., Graham, D., & Eppe, G. (2024). Thiol-polyethylene glycol-folic acid (HS-PEG-FA) induced aggregation of Au@Ag nanoparticles: a SERS and extinction UV–Vis spectroscopy combined study. *Spectrochimica Acta - Part A: Molecular and Biomolecular Spectroscopy*, *322*, Article 124848. Advance online publication. https://doi.org/10.1016/j.saa.2024.124848

Vis extinction spectra are similar to the spectrum in the absence of PEG (Figure 1a). The only noticeable difference is a slight red-shift of the LSPR at high PEG concentration due to a change in the refractive index at the surface of the NPs, confirming the anchoring of the PEG chains on the Ag surface through the thiol function.

We used the ratio of the extinction at 630 nm and of the extinction at the LSPR of the Au@Ag NPs to quantify the extent of the aggregation. The ratio of extinctions was arbitrarily set to 1 for the condition inducing the strongest aggregation to allow a full comparison of all conditions. The ratio of extinction at 630 nm (related to aggregates) with respect to the extinction at 395 nm (maximum of extinction of the non-aggregated Au@Ag NPs) reaches a maximum at a concentration of incubated PEG of roughly $4x10^{-7}$ M (Figure 2a). Therefore, some concentrations of PEG seem to be detrimental to the stability of the NPs as evidenced by an increase of the aggregation.

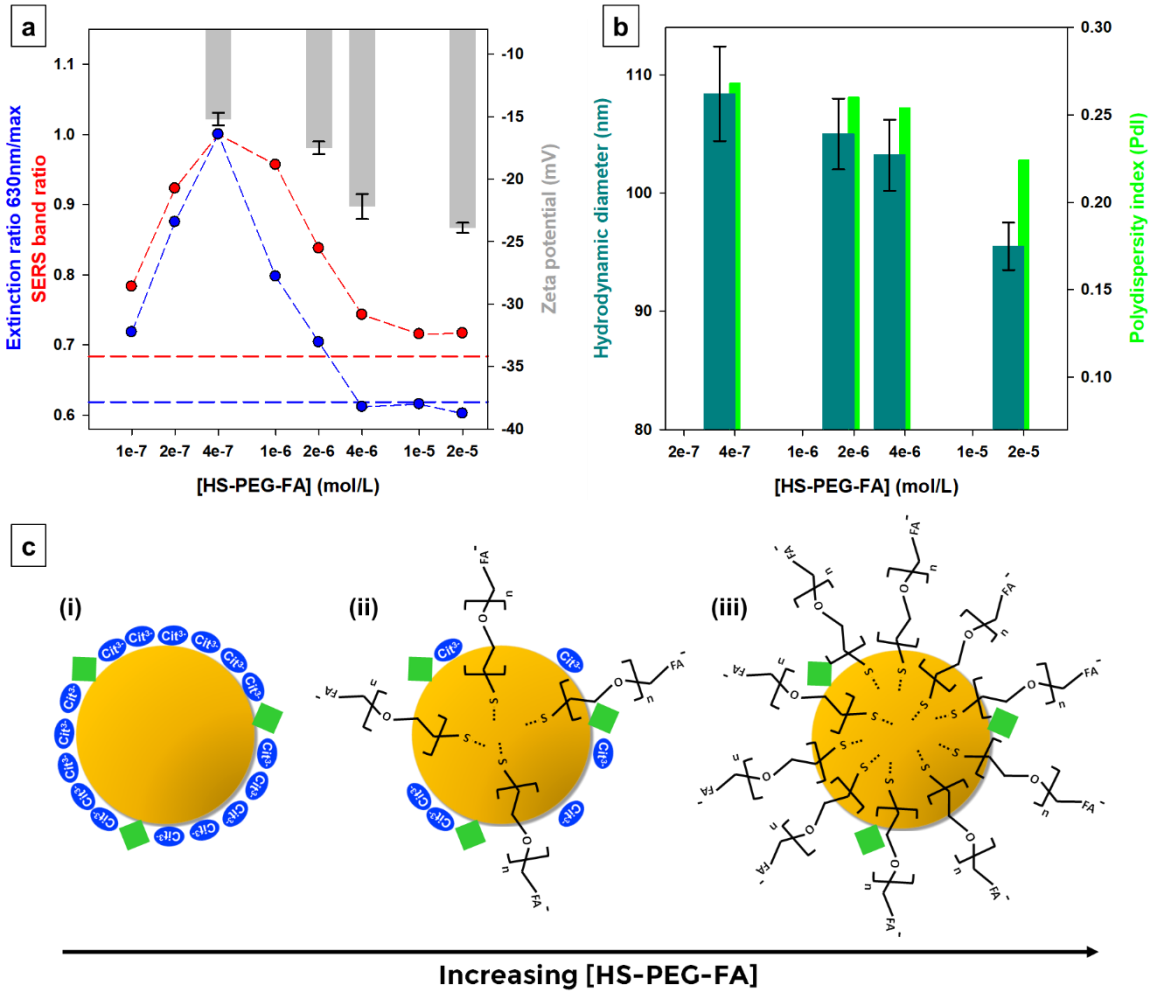

Figure 2. (a) Evolution of the ratio between the extinction at 630 nm and at the extinction maximum (blue dots) and of the SERS intensity ratio between the bands at 1587 and 1615 cm^{-1} (red dots) as a function of the concentration of HS-PEG-FA. The blue and red dashed lines indicate the values of extinction ratio and SERS band ratio when no HS-PEG-FA is present, respectively. Zeta potential values at some HS-PEG-FA concentration are also represented with grey bars. (b) Average hydrodynamic diameter (and standard deviation from three replicates) and associated polydispersity index measured for some HS-PEG-FA concentration. (c) Illustration of the progressive replacement of citrate

ions by HS-PEG-FA chains upon increasing HS-PEG-FA concentration. Green squares and blue ellipses represent MGITC molecules and citrate ions, respectively. Situation referred to as "(ii)" is believed to be the situation when HS-PEG-FA is $4x10^{-7}$ M, inducing aggregation of the NPs.

At concentrations lower than $4x10^{-7}$ M, aggregation gradually increases with the PEG concentration when compared to the starting situation (no PEG), but the aggregation is not maximal (Figure 2a). At concentrations higher than $4x10^{-7}$ M, the system regains progressively its stability as the PEG concentration increases and at $4x10^{-6}$ M the extinction ratio is similar to the starting situation (no PEG), indicating that there is no aggregation (Figure 2a). This is confirmed in Figure 1a which shows the UV-Vis extinction spectra of MGITC-functionalised Au@Ag NPs in the absence of PEG and in the presence of PEG at $4x10^{-7}$ and $4x10^{-6}$ M. The extinction at higher wavelength for the PEG concentration of $4x10^{-7}$ M clearly indicates an increased aggregation compared to the situation without PEG or compared to the situation with PEG at $4x10^{-6}$ M. Simultaneously to these experiments, we also used tools developed in a previous study to measure the actual amount of PEG linked to the NPs as a function of the incubated PEG concentration [29]. With these tools, we evaluated that a concentration of $4x10^{-7}$ M corresponds to around 650 chains of PEG per NP while a concentration of $4x10^{-6}$ M corresponds to around 4600 chains per NP. Full surface coverage is achieved around $2x10^{-5}$ M of PEG and corresponds to ≈ 11000 chains per NP.

To gain further insight into the destabilisation process, we measured the zeta potential at various PEG concentrations (Figure 2a). Before adding any PEG (only MGITC present), the zeta potential of the NPs is -23 (± 1) mV. It is not very different from the bare NPs (-26 ± 1 mV) since the number of MGITC molecules used for functionalisation is low (Figure 2c, situation (i)). At $4x10^{-7}$ M of PEG, the zeta potential is -15.2 (± 0.5) mV. The zeta potential slightly decreases to -17.5 (± 0.5) mV at $2x10^{-6}$ M of PEG and further decreases to -22.2 (± 1) mV at $4x10^{-6}$ M. At very large concentrations of PEG ($2x10^{-5}$ M), the zeta potential is -23.9 (± 0.4) mV. These results strongly suggest that the system is electrostatically destabilised at low PEG concentration ($4x10^{-7}$ M) and therefore that the corresponding number of PEG chains are not able to counterbalance the loss of stabilisation induced by the removal of citrate ions during PEG grafting (Figure 2a). Similar behaviour has been observed by Wang and co-workers when adding HS-PEG-OCH_3 chains on Au NPs [39]. Indeed, thiolated-PEG chains are bulky and displace several citrate ions per single PEG chain [39]–[41] (Figure 2c, situation (ii)). However, each chain of HS-PEG-FA only brings a single negative charge (carboxylate function on folic acid at the chain end). Below 650 PEG chains, citrate ions are still present in sufficient amounts to provide electrostatic repulsion (Figure 2c, situation (i)), while above 650 PEG chains, the steric stabilisation provided by the polymeric chains start to take place alongside the electrostatic repulsion (Figure 2c, situation (iii)).

Additionally, the extent of the aggregation can be followed by measuring the hydrodynamic diameter (and associated polydispersity index, PdI) of the NPs in different conditions. The average hydrodynamic diameter at a PEG concentration of $4x10^{-7}$ M is 108.4 (± 4) nm with a

PdI of 0.268, and both values progressively decrease when the PEG concentration is increased (Figure 2b). When a large excess of PEG is present (concentration of $2x10^{-5}$ M), the hydrodynamic diameter is 95.5 (± 2) nm with a PdI of 0.224. This observed difference is consistent with a different degree of aggregation of the Au@Ag NPs between the two PEG concentrations as already evidenced with other techniques. At low PEG concentration ($4x10^{-7}$ M), aggregation occurs and slightly shifts the population of NPs toward a larger average hydrodynamic diameter because a larger part of the initial NPs is in the form of aggregates and larger nanostructures scatter light more efficiently [42]. This is also confirmed by a larger polydispersity index indicating that the NPs size population is larger. However, at high PEG concentration ($2x10^{-5}$ M), the average hydrodynamic diameter is at a lower value because there are no additional aggregates in the solution. This is also confirmed by the PdI that is comparable to the PdI of NPs without PEG (0.236).

3.2. *SERS study*

The evolution of the SERS spectra of MGITC-functionalised NPs with increasing concentrations of HS-PEG-FA was then investigated. Spectra were normalised to the most intense band of MGITC at 1615 cm^{-1} to rule out the influence of the absolute intensity. Area normalised spectra (constant amount of MGITC) were also investigated and led to the same conclusions. Area normalisation was possible because MGITC molecules were not displaced from the surface of the Au@Ag NPs even when a large excess of PEG was used (Figure S1). For some PEG concentrations, strong spectral modifications are observed (Figure 1b). Notably, the most obvious spectral change is the increase, for some PEG concentrations, of the band at 1587 cm^{-1}. In the following discussion, we used the intensity ratio of the 1587 to the 1615 cm^{-1} bands to further investigate the influence of PEG on the spectral shape of MGITC.

The SERS intensity ratio between the bands at 1587 and 1615 cm^{-1} was also normalised to 1 for the highest value to allow comparison with UV-Vis extinction data. The SERS bands ratio follows a similar trend across the whole PEG concentration range as the extinction ratio observed with UV-Vis, with a maximum observed at a PEG concentration of $4x10^{-7}$ M (Figure 2a). This similar trend indicates that the aggregation that occurs when the amount of PEG is too low influences the spectral signature of MGITC. Figure 3 shows the SERS spectrum of MGITC obtained at a PEG concentration of $4x10^{-7}$ M (strongest destabilisation) and at $4x10^{-6}$ M (no destabilisation). At $4x10^{-6}$ M, the spectrum is similar to the spectrum of MGITC in the absence of any PEG, while at $4x10^{-7}$ M strong spectral changes are observed and not only for the band at 1587 cm^{-1}.

Verdin, A., Malherbe, C., Sloan-Dennison, S., Faulds, K., Graham, D., & Eppe, G. (2024). Thiol-polyethylene glycol-folic acid (HS-PEG-FA) induced aggregation of Au@Ag nanoparticles: a SERS and extinction UV–Vis spectroscopy combined study. *Spectrochimica Acta - Part A: Molecular and Biomolecular Spectroscopy*, *322*, Article 124848. Advance online publication. https://doi.org/10.1016/j.saa.2024.124848

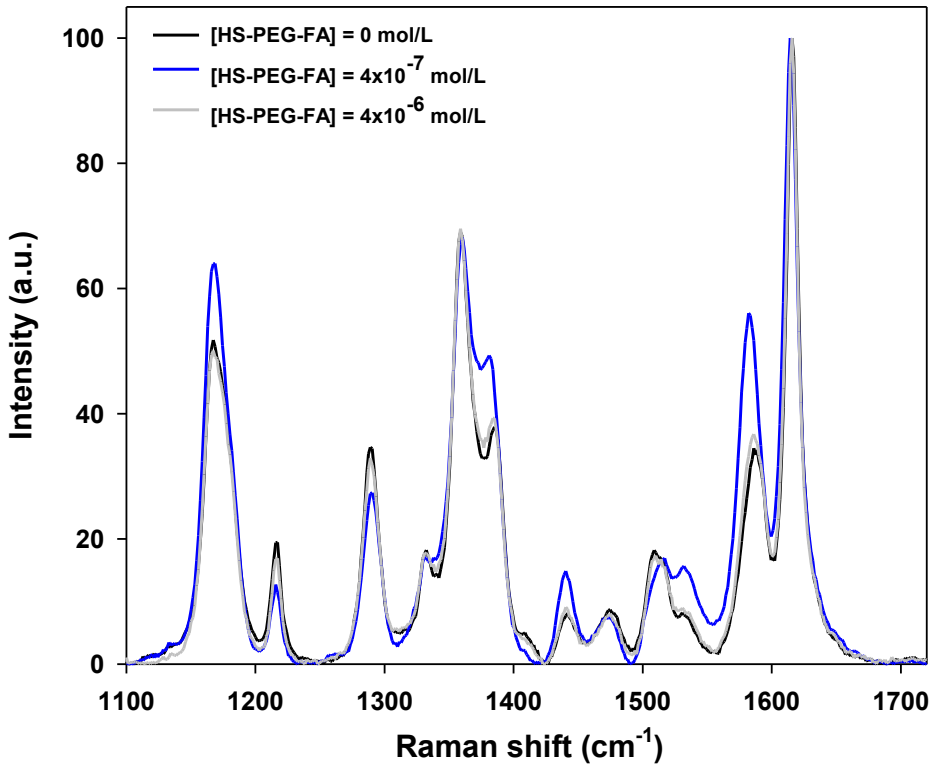

Figure 3. Normalised SERS spectrum of MGITC-functionalised Au@Ag NPs obtained at 532 nm for various concentration of HS-PEG-FA: 0 M (black), $4x10^{-7}$ M (blue) and $4x10^{-6}$ M (grey).

Final evidence regarding the link between aggregation and spectral shape of MGITC, we performed via time-lapse measurements of both band ratio in SERS and extinction ratio in UV-Vis after incubation of either $4x10^{-7}$ M or $4x10^{-6}$ M of HS-PEG-FA.

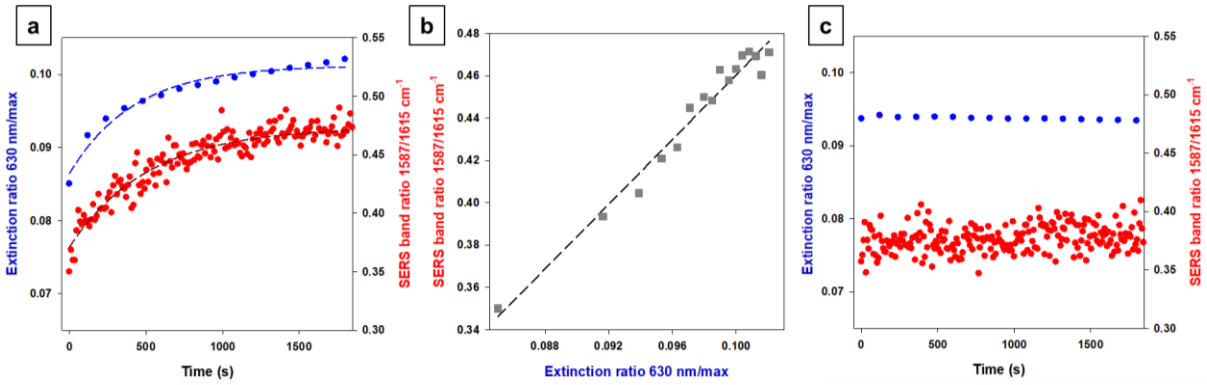

Figure 4. (a) Temporal evolution of the ratio between the extinction at 630 nm and at the position of the extinction maximum (blue dots) and of the SERS intensity ratio between the 1587 and 1615 cm^{-1} bands (red dots) after incubation with HS-PEG-FA at $4x10^{-7}$ M. (b) SERS intensity ratio between the 1587 and 1615 cm^{-1} bands as a function of the ratio between the extinction at 630 nm and at the position of the extinction maximum obtained for the same time points. R^2 of 0.96 shows the linear correlation between both quantities. (c) Temporal evolution of the ratio between the extinction at 630 nm and at the position of the extinction maximum (blue dots) and of the SERS intensity ratio between the 1587 and 1615 cm^{-1} bands (red dots) after incubation with HS-PEG-FA at $4x10^{-6}$ M.

Verdin, A., Malherbe, C., Sloan-Dennison, S., Faulds, K., Graham, D., & Eppe, G. (2024). Thiol-polyethylene glycol-folic acid (HS-PEG-FA) induced aggregation of Au@Ag nanoparticles: a SERS and extinction UV–Vis spectroscopy combined study. *Spectrochimica Acta - Part A: Molecular and Biomolecular Spectroscopy*, *322*, Article 124848. Advance online publication. https://doi.org/10.1016/j.saa.2024.124848

When $4x10^{-7}$ M of PEG was incubated with the NPs, both quantities have very similar temporal evolution with fast growth at the start and with a plateau reached after ≈ 1000 s, indicating that the system is stabilised later on (Figure 4a). This mirror temporal evolution is confirmed by plotting, for the same incubation time, the SERS band ratio versus the extinction ratio (Figure 4b). We obtained a high determination coefficient ($R^2 = 0.96$) clearly indicating that the spectral shape of MGITC and aggregation of the NPs are intrinsically connected. These observations are consistent with previous reports by Cheng and co-workers [43], [44]. When the PEG concentration was $4x10^{-6}$ M, no SERS spectral change or extinction ratio change was observed over time as evidenced in Figure 4c.

We also observed that the destabilisation described above was not influenced by the presence of MGITC at the surface of the NPs. Similar experiments were performed with bare Au@Ag NPs and only the extinction ratio could be followed, since no Raman reporter was present. We observed that the largest destabilisation was induced at the same PEG concentration as for MGITC-functionalised NPs (Figure 5). In this case however, the difference in aggregation between the situation with no PEG and the situation at [PEG] = $4x10^{-7}$ M is larger. This is because the starting bare Au@Ag NPs are in an even lower aggregation state compared to the MGITC-functionalised NPs. Indeed, labelling with MGITC even at very low concentrations unavoidably induces slight increase in extinction at higher wavelength. These results further confirm the mechanism discussed above regarding the destabilisation of the NPs at certain PEG concentrations (Figure 2c).

Verdin, A., Malherbe, C., Sloan-Dennison, S., Faulds, K., Graham, D., & Eppe, G. (2024). Thiol-polyethylene glycol-folic acid (HS-PEG-FA) induced aggregation of Au@Ag nanoparticles: a SERS and extinction UV–Vis spectroscopy combined study. *Spectrochimica Acta - Part A: Molecular and Biomolecular Spectroscopy*, *322*, Article 124848. Advance online publication. https://doi.org/10.1016/j.saa.2024.124848

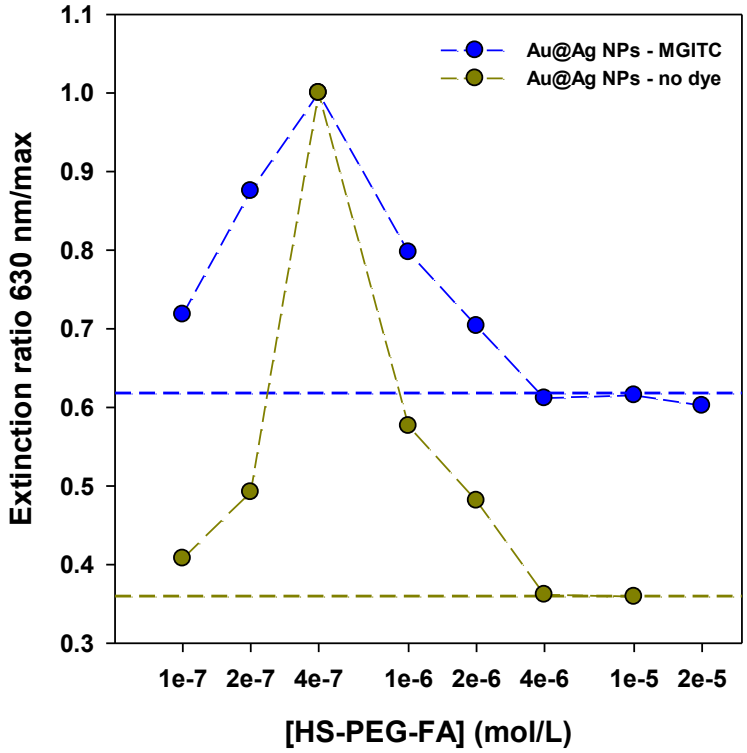

Figure 5. Evolution of the ratio between the extinction at 630 nm and at the maximum of extinction for MGITC-functionalised NPs (blue dots) and for bare Au@Ag NPs (dark yellow dots) as a function of the concentration of HS-PEG-FA. The dashed lines indicate the values of extinction ratio when no HS-PEG-FA is present.

3.3. Spectral analysis of MGITC in the aggregated state

In this section, we try to rationalise the spectral changes of MGITC in the aggregated state. Detailed analysis of the SERS spectra before and after aggregation induced by low amounts of HS-PEG-FA was performed. Spectra were normalised to the band at 1615 cm^{-1} for comparison purpose (Figure 6a). Area normalisation led to similar observations. This band corresponds to the N-phenyl + C-C stretching mode [45]. The major spectral changes associated with the aggregation are: large intensity increase of the 1587 cm^{-1} band (in-plane phenyl ring stretching and bending), intensity increase of the 1440 cm^{-1} band (N-Me_2 rocking and bending), intensity increase of the 1385 cm^{-1} band (N-phenyl symmetric stretching), slight intensity decrease of the 1358 cm^{-1} band (N-phenyl antisymmetric stretching), intensity decrease of the 1290 cm^{-1} band (out-of-plane ring stretching), intensity increase of the 1170 cm^{-1} band (C-H in plane stretching), large intensity increase of the 907 cm^{-1} band (ring skeletal vibration), slight intensity decrease of the 793 cm^{-1} band (C-H out-of-plane stretching). Also, an obvious change in the bands between 1500 and 1560 cm^{-1} is observed however these bands could not be accurately assigned based on the existing literature.

Moreover, some frequency shifts are observed. The main band initially at 1615 cm^{-1} slightly shifts to 1613 cm^{-1} and the band at 1587 cm^{-1} shifts toward 1583 cm^{-1} (Figure 6d). The band at 1291 cm^{-1} shifts to 1289 cm^{-1} (Figure 6b). The first two bands are related to the in-plane ring

stretching of the aromatic rings of MGITC, and the third is related to out-of-plane ring stretching. Bands associated with N-phenyl vibrations (1358 and 1385 cm^{-1}) shift closer to each other: 1358 cm^{-1} shifts to 1360 cm^{-1} and 1385 cm^{-1} shifts to 1382.5 cm^{-1} (Figure 6c). Changes in the frequency of vibration of certain modes indicate a modification of the bond strength that could suggest a different electronic environment in this case since the molecule remains the same.

The spectral changes described above suggest that the molecule adopts a more perpendicularly-oriented conformation (or less tilted, since MGITC is believed to be in a tilted conformation while anchored on the surface by the ITC function [45], [46]) to the surface after aggregation. Indeed, vibrational modes that vibrate in the plane of the molecule, namely the 1587, 1385, 1170, and 907 cm^{-1} modes all show an intensity increase during aggregation. In SERS, the amplified electric field is generally considered to be perpendicular to the surface of the NPs. Therefore, a perfectly vertically-oriented molecule will see its vibrational modes in the plane of the molecule (and therefore aligned with the electric field) preferentially amplified [47]. This is what we observe for MGITC after aggregation. On the other hand, vibrational modes that vibrate outside of the plane of the molecule such as the 1290 or 793 cm^{-1} modes are weakened during the aggregation. This is also consistent with a more vertically-oriented conformation of MGITC since these modes will be less aligned with the amplified electric field than before aggregation. Frequency shifts of several bands related to phenyl rings could be evidence for increased inter-molecular interactions probably through π- π stacking. Indeed, stacking will slightly increase the electronic density in the aromatic rings of MGITC, which will be detrimental to the strength of the bonds under vibration since the supplementary electronic density will be located in anti-bonding orbitals. The strength of the bonds will therefore slightly decrease and induce a shift toward lower wavenumbers in the vibrational spectrum (blue shift). On the other hand, Raman bands related to C-H vibrations on the aromatic rings (1170 and 793 cm^{-1}) do not exhibit any significant shift.

Based on these observations, we hypothesized that MGITC molecules adsorbed on distinct NPs are forced to interact more strongly with each other when the distance between NPs is decreased through aggregation, resulting in a more vertically aligned conformation of MGITC to increase the surface of the inter-molecular interactions (more favourable stacking). Similar effects were evidenced recently for crystal violet by Fabris et al [48]. It has also been reported that for some dyes, such as cyanines, aggregation of the NPs can lead to the formation of molecular aggregates through π-π stacking, bridging the nanoparticles together [43], [44], [49]. Such molecular aggregates are characterised by a particular alignment of several dye molecules (most of the time two molecules forming dimers) with respect to each other [50]. This kind of phenomenon is known to induce band shifts and changes of band intensity ratios in the Raman spectra of the aggregated dyes [51]. Therefore, a similar mechanism of molecular aggregation of MGITC inside the NP aggregates could also be the cause of the observed spectral changes.

Verdin, A., Malherbe, C., Sloan-Dennison, S., Faulds, K., Graham, D., & Eppe, G. (2024). Thiol-polyethylene glycol-folic acid (HS-PEG-FA) induced aggregation of Au@Ag nanoparticles: a SERS and extinction UV–Vis spectroscopy combined study. *Spectrochimica Acta - Part A: Molecular and Biomolecular Spectroscopy*, *322*, Article 124848. Advance online publication. https://doi.org/10.1016/j.saa.2024.124848

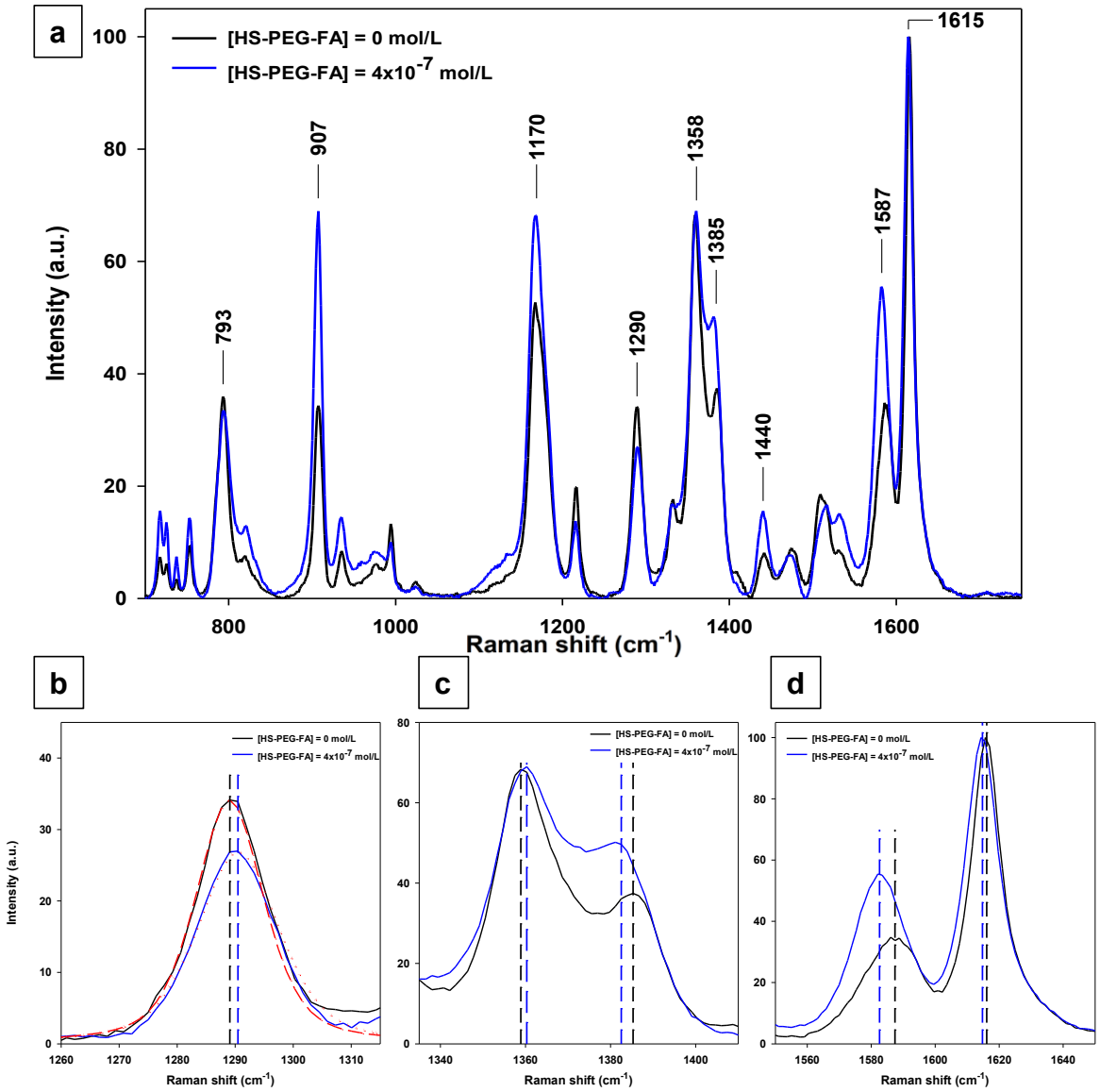

Figure 6. (a) SERS spectrum obtained for MGITC-functionalised NPs in HEPES buffer in the absence of HS-PEG-FA (black) and in the presence of HS-PEG-FA at a concentration of $4x10^{-7}$ M (blue). The main bands used for spectral analysis are highlighted. Illustration of several band shifts after aggregation of the system: (b) Zoom on the 1291 cm^{-1} band shifting to 1289 cm^{-1}. (c) Zoom on the bands associated to N-phenyl stretching shifting toward each other (1358 to 1360 cm^{-1} and 1385 to 1382.5 cm^{-1}). (d) Zoom on the 1615 and 1587 cm^{-1} bands shifting to 1613 and 1583 cm^{-1}, respectively.

We further analysed the spectral characteristics of the NP aggregates by isolating and concentrating them using centrifugation at low speed (900 RCF). The isolated fraction exhibited a strong brown coloration, in contrast with the bright orange colour of the Au@Ag colloid. UV-Vis extinction spectrum of the isolated fraction show that NPs aggregates exhibit a broad main absorption band located at 395 nm with a strong second broad band located at ≈ 700 nm (Figure 7a). This is consistent with the aggregated nature of this fraction since larger nanostructures are present in the solution, leading to the appearance of a new plasmonic band at longer wavelength. The SERS spectrum of the isolated fraction (normalised to the band at

1615 cm^{-1}) shows major differences with the spectrum of the non-aggregated NPs. We observe a massive intensity increase of the band at 1583 cm^{-1}, and the bands at 1170 and 1383 cm^{-1} also increase in intensity (Figure 7b). These observations are consistent with the spectral changes that we described earlier (without isolation of the aggregates). More importantly, when we computed the difference in the SERS spectrum between conditions with PEG at $4x10^{-7}$ M and no PEG, we obtained a spectral shape that matches nicely with the experimental spectrum measured for the isolated aggregates (Figure 7c). This is definitive proof that the spectral changes observed are caused by the aggregates, and that the MGITC molecules adopt a different conformation in the aggregates than on the non-aggregated NPs. This also indicates that the aggregates produce much brighter SERS than the non-aggregated NPs because only a very small fraction of the NPs population is in the aggregate form (observed in the changes in the UV-Vis extinction spectra which are not very pronounced even at [HS-PEG-FA] = $4x10^{-7}$ M), but they strongly contribute to the overall SERS spectra. These results emphasize the necessity of properly studying the stability of NPs and understanding the effect of aggregation (even a low degree of aggregation) since they can have a dramatic effect on the SERS spectra.

Verdin, A., Malherbe, C., Sloan-Dennison, S., Faulds, K., Graham, D., & Eppe, G. (2024). Thiol-polyethylene glycol-folic acid (HS-PEG-FA) induced aggregation of Au@Ag nanoparticles: a SERS and extinction UV–Vis spectroscopy combined study. *Spectrochimica Acta - Part A: Molecular and Biomolecular Spectroscopy*, *322*, Article 124848. Advance online publication. https://doi.org/10.1016/j.saa.2024.124848

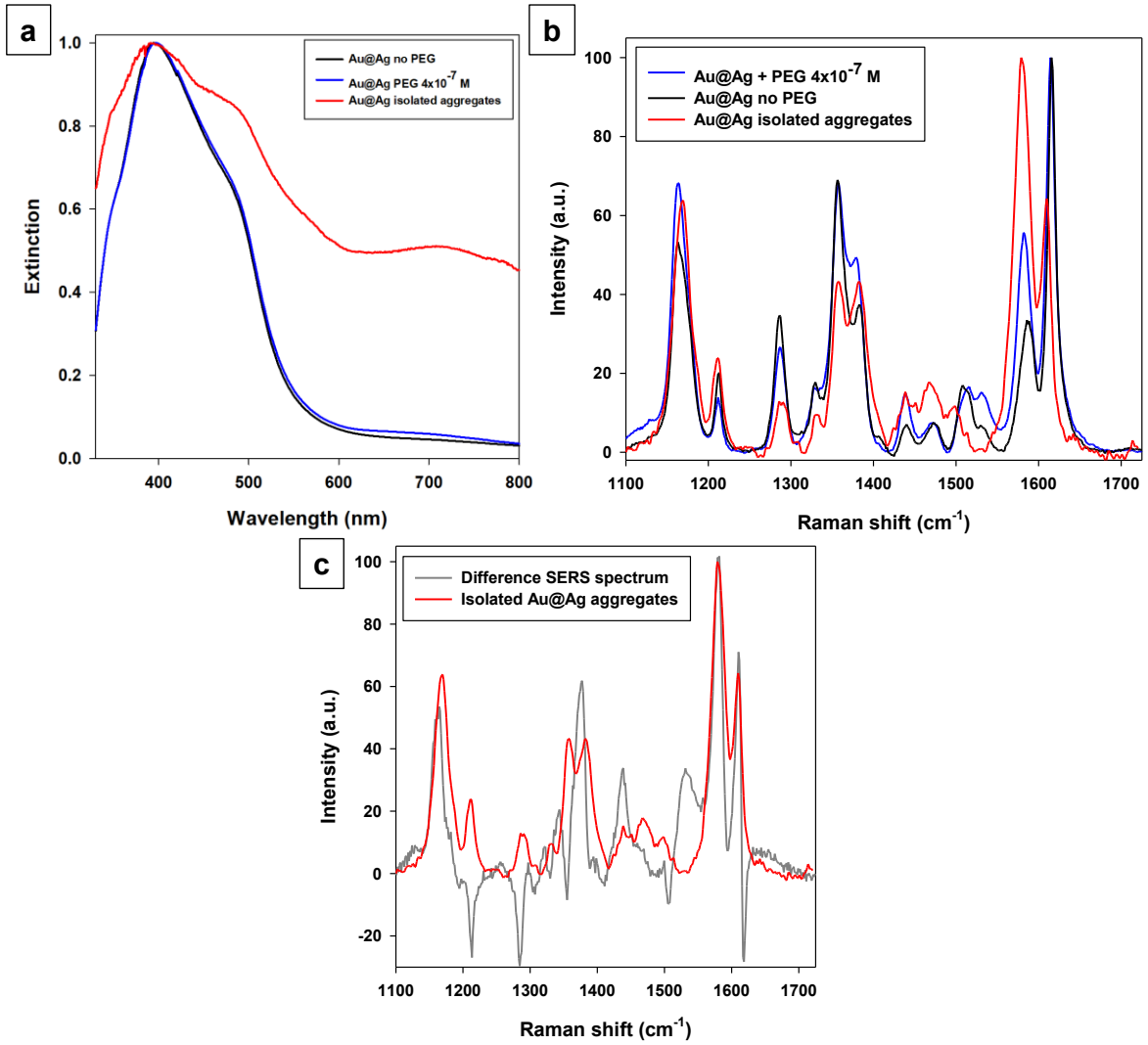

Figure 7. (a) UV-Vis extinction spectrum of Au@Ag NPs labelled with MGITC in the absence of HS-PEG-FA (black), in the presence of HS-PEG-FA at $4x10^{-7}$ M (blue) and of the isolated aggregates after centrifugation of the Au@Ag NPs incubated with HS-PEG-FA at $4x10^{-7}$ M (red). (b) SERS spectrum of Au@Ag NPs labelled with MGITC in the absence of HS-PEG-FA (black), in the presence of HS-PEG-FA at $4x10^{-7}$ M (blue) and of the isolated aggregates after centrifugation of the Au@Ag NPs incubated with HS-PEG-FA at $4x10^{-7}$ M (red). (c) Computed difference SERS spectrum between the conditions at [HS-PEG-FA] = $4x10^{-7}$ M and at [HS-PEG-FA] = 0 M (grey), and experimental SERS spectrum measured on the isolated Au@Ag aggregates after centrifugation of the Au@Ag NPs incubated with HS-PEG-FA at $4x10^{-7}$ M (red).

4. Conclusion

In conclusion, this paper highlights the detrimental impact of certain amounts of thiolated-PEG chains on the stability of Au@Ag NPs, which lead to slight aggregation and influence the spectral signature of Raman-reporter molecules. The study explores the origin of PEG-induced aggregation through various techniques, attributing it to electrostatic destabilisation. The present work also examines the effect of aggregation on the SERS spectrum of MGITC, revealing differences in spectral shape between aggregated and non-aggregated NPs. The findings underscore the importance of considering even low degrees of aggregation when

studying Raman-reporter molecule spectral shapes, especially in approaches using SERS nanotags and relying on spectrum fitting, as aggregation-induced changes may affect the analysis results.

These stability issues have significant implications for the practical applications of SERS nanotags. In biomedical imaging and diagnostics, uncontrolled aggregation can lead to inconsistent and unreliable results, potentially compromising the accuracy of disease detection and monitoring [19]. Similarly, in environmental sensing applications where SERS nanotags may be used [52], the altered spectral signatures that may be due to aggregation can result in false positives or negatives, compromising the detection of pollutants for example. Therefore, ensuring the stability of SERS nanotags in various conditions is crucial for maintaining the reliability and accuracy of these advanced analytical techniques in real-world applications. Moreover, uncontrolled aggregation could lead to significant loss of sensitivity in the detection of the nanotags if the optical properties of the aggregated nanotags are less compatible with the wavelength used for analysis [53]. This study serves as a critical reminder for researchers to meticulously consider nanoparticle stability in the design and deployment of SERS-based technologies.

References

[1] J. Krajczewski, K. Kołątaj, and A. Kudelski, “Plasmonic nanoparticles in chemical analysis,” *RSC Adv.*, vol. 7, no. 28, pp. 17559–17576, 2017, doi: 10.1039/C7RA01034F.

[2] W. Q. Lim and Z. Gao, “Plasmonic nanoparticles in biomedicine,” *Nano Today*, vol. 11, no. 2, pp. 168–188, 2016, doi: https://doi.org/10.1016/j.nantod.2016.02.002.

[3] J. Liu *et al.*, “Recent Advances of Plasmonic Nanoparticles and their Applications,” *Materials*, vol. 11, no. 10. 2018, doi: 10.3390/ma11101833.

[4] J. Olson, S. Dominguez-Medina, A. Hoggard, L.-Y. Wang, W.-S. Chang, and S. Link, “Optical characterization of single plasmonic nanoparticles,” *Chem. Soc. Rev.*, vol. 44, no. 1, pp. 40–57, 2015, doi: 10.1039/C4CS00131A.

[5] I. Pastoriza-Santos, C. Kinnear, J. Pérez-Juste, P. Mulvaney, and L. M. Liz-Marzán, “Plasmonic polymer nanocomposites,” *Nat. Rev. Mater.*, vol. 3, no. 10, pp. 375–391, 2018, doi: 10.1038/s41578-018-0050-7.

[6] H. Duan, Y. Yang, Y. Zhang, C. Yi, Z. Nie, and J. He, “What is next in polymer-grafted plasmonic nanoparticles?,” *Giant*, vol. 4, p. 100033, 2020, doi: https://doi.org/10.1016/j.giant.2020.100033.

[7] A. Amirjani and E. Rahbarimehr, “Recent advances in functionalization of plasmonic nanostructures for optical sensing,” *Microchim. Acta*, vol. 188, no. 2, p. 57, 2021, doi: 10.1007/s00604-021-04714-3.

[8] L. E. Strong and J. L. West, “Thermally responsive polymer–nanoparticle composites for biomedical applications,” *WIREs Nanomedicine and Nanobiotechnology*, vol. 3, no. 3, pp. 307–317, May 2011, doi: https://doi.org/10.1002/wnan.138.

[9] M. Ghorbani and H. Hamishehkar, “Redox and pH-responsive gold nanoparticles as a new platform for simultaneous triple anti-cancer drugs targeting,” *Int. J. Pharm.*, vol. 520, no. 1, pp. 126–138, 2017, doi: https://doi.org/10.1016/j.ijpharm.2017.02.008.

[10] S. Mahalunkar *et al.*, “Functional design of pH-responsive folate-targeted polymer-coated gold nanoparticles for drug delivery and in vivo therapy in breast cancer,” *Int. J. Nanomedicine*, vol. 14, no. null, pp. 8285–8302, Oct. 2019, doi: 10.2147/IJN.S215142.

[11] M. Theodosiou, N. Boukos, E. Sakellis, M. Zachariadis, and E. K. Efthimiadou, “Gold nanoparticle decorated pH-sensitive polymeric nanocontainers as a potential theranostic agent,” *Colloids Surfaces B Biointerfaces*, vol. 183, p.

110420, 2019, doi: https://doi.org/10.1016/j.colsurfb.2019.110420.

[12] M. Zubair Iqbal, I. Ali, W. S. Khan, X. Kong, and E. Dempsey, "Reversible self-assembly of gold nanoparticles in response to external stimuli," *Mater. Des.*, vol. 205, p. 109694, 2021, doi: https://doi.org/10.1016/j.matdes.2021.109694.

[13] Y. Ofir, B. Samanta, and V. M. Rotello, "Polymer and biopolymer mediated self-assembly of gold nanoparticles," *Chem. Soc. Rev.*, vol. 37, no. 9, pp. 1814–1825, 2008, doi: 10.1039/B712689C.

[14] S. Siddique and J. C. L. Chow, "Gold Nanoparticles for Drug Delivery and Cancer Therapy," *Applied Sciences*, vol. 10, no. 11. 2020, doi: 10.3390/app10113824.

[15] J. Langer *et al.*, "Present and Future of Surface-Enhanced Raman Scattering," *ACS Nano*, 2019, doi: 10.1021/acsnano.9b04224.

[16] G. Barbillon, "Latest novelties on plasmonic and non-plasmonic nanomaterials for SERS sensing," *Nanomaterials*, vol. 10, no. 6. pp. 1–17, 2020, doi: 10.3390/nano10061200.

[17] Y. Wang and S. Schlücker, "Rational design and synthesis of SERS labels," *Analyst*, vol. 138, no. 8, pp. 2224–2238, 2013, doi: 10.1039/c3an36866a.

[18] Y. Wang, B. Yan, and L. Chen, "SERS Tags: Novel Optical Nanoprobes for Bioanalysis," *Chem. Rev.*, vol. 113, no. 3, pp. 1391–1428, Mar. 2013, doi: 10.1021/cr300120g.

[19] H. Liu, X. Gao, C. Xu, and D. Liu, "SERS Tags for Biomedical Detection and Bioimaging," *Theranostics*, vol. 12, no. 4, pp. 1870–1903, 2022, doi: 10.7150/thno.66859.

[20] M. J. Oliveira *et al.*, "Microfluidic SERS devices: brightening the future of bioanalysis," *Discov. Mater.*, vol. 2, no. 1, p. 12, 2022, doi: 10.1007/s43939-022-00033-3.

[21] L. Fabris, "SERS Tags: The Next Promising Tool for Personalized Cancer Detection?," *ChemNanoMat*, vol. 2, no. 4, pp. 249–258, Apr. 2016, doi: https://doi.org/10.1002/cnma.201500221.

[22] L. Shi *et al.*, "Effects of polyethylene glycol on the surface of nanoparticles for targeted drug delivery," *Nanoscale*, vol. 13, no. 24, pp. 10748–10764, 2021, doi: 10.1039/D1NR02065J.

[23] E. Harrison *et al.*, "A comparison of gold nanoparticle surface co-functionalization approaches using Polyethylene Glycol (PEG) and the effect on stability, non-specific protein adsorption and internalization," *Mater. Sci. Eng. C*, vol. 62, pp. 710–718, 2016, doi: https://doi.org/10.1016/j.msec.2016.02.003.

[24] K. Partikel *et al.*, "Effect of nanoparticle size and PEGylation on the protein corona of PLGA nanoparticles," *Eur. J. Pharm. Biopharm.*, vol. 141, pp. 70–80, 2019, doi: https://doi.org/10.1016/j.ejpb.2019.05.006.

[25] Y. Xue, X. Li, H. Li, and W. Zhang, "Quantifying thiol-gold interactions towards the efficient strength control," *Nat. Commun.*, vol. 5, no. 1, p. 4348, 2014, doi: 10.1038/ncomms5348.

[26] T. Bürgi, "Properties of the gold-sulphur interface: from self-assembled monolayers to clusters," *Nanoscale*, vol. 7, no. 38, pp. 15553–15567, 2015, doi: 10.1039/c5nr03497c.

[27] D. B. Knowles, A. S. LaCroix, N. F. Deines, I. Shkel, and M. T. Record, "Separation of preferential interaction and excluded volume effects on DNA duplex and hairpin stability," *Proc. Natl. Acad. Sci.*, vol. 108, no. 31, pp. 12699–12704, Aug. 2011, doi: 10.1073/pnas.1103382108.

[28] U. Dahal and E. E. Dormidontova, "Chain Conformation and Hydration of Polyethylene Oxide Grafted to Gold Nanoparticles: Curvature and Chain Length Effect," *Macromolecules*, vol. 53, no. 19, pp. 8160–8170, Oct. 2020, doi: 10.1021/acs.macromol.0c01499.

[29] A. Verdin, S. Sloan-Dennison, C. Malherbe, D. Graham, and G. Eppe, "SERS nanotags for folate receptor α detection at the single cell level: discrimination of overexpressing cells and potential for live cell applications," *Analyst*, vol. 147, no. 14, pp. 3328–3339, 2022, doi: 10.1039/d2an00706a.

[30] M. Scaranti, E. Cojocaru, S. Banerjee, and U. Banerji, "Exploiting the folate receptor α in oncology," *Nat. Rev. Clin. Oncol.*, vol. 17, no. 6, pp. 349–359, 2020, doi: 10.1038/s41571-020-0339-5.

[31] A. Cheung *et al.*, "Targeting folate receptor alpha for cancer treatment," *Oncotarget*, vol. 7, no. 32, pp. 52553–52574, 2016, doi: 10.18632/oncotarget.9651.

[32] S. Chen, M. Lv, J. Fan, Y. Huang, G. Liang, and S. Zhang, "Bioorthogonal surface-enhanced Raman scattering flower-like nanoprobe with embedded standards for accurate cancer cell imaging," *Anal. Chim. Acta*, vol. 1246, p. 340895, 2023, doi: 10.1016/j.aca.2023.340895.

[33] A. M. Fales, B. M. Crawford, and T. Vo-Dinh, "Folate Receptor-Targeted Theranostic Nanoconstruct for Surface-Enhanced Raman Scattering Imaging and Photodynamic Therapy," *ACS Omega*, vol. 1, no. 4, pp. 730–735, 2016, doi: 10.1021/acsomega.6b00176.

[34] P. Kedarisetti *et al.*, "Enrichment and ratiometric detection of circulating tumor cells using PSMA- and folate receptor-targeted magnetic and surface-enhanced Raman scattering nanoparticles," in *Biomedical Optics Express*, vol. 11, no. 11, vol. 11, no. 11: Opt. Express, 2020, p. 6211.

[35] T. Köker *et al.*, "Cellular imaging by targeted assembly of hot-spot SERS and photoacoustic nanoprobes using split-fluorescent protein scaffolds," *Nat. Commun.*, vol. 9, no. 1, p. 607, 2018, doi: 10.1038/s41467-018-03046-w.

[36] A. Kapara, V. G. Brunton, D. Graham, and K. Faulds, "Characterisation of estrogen receptor alpha (ERα) expression in breast cancer cells and effect of drug treatment using targeted nanoparticles and SERS," *Analyst*, vol. 145, no. 22, pp. 7225–7233, 2020, doi: 10.1039/d0an01532f.

[37] A. A. Leventi *et al.*, "New Model for Quantifying the Nanoparticle Concentration Using SERS Supported by Multimodal Mass Spectrometry," *Anal. Chem.*, vol. 95, no. 5, pp. 2757–2764, Feb. 2023, doi: 10.1021/acs.analchem.2c03779.

[38] A. Verdin, C. Malherbe, W. H. Müller, V. Bertrand, and G. Eppe, "Multiplex micro-SERS imaging of cancer-related markers in cells and tissues using poly(allylamine)-coated Au@Ag nanoprobes," *Anal. Bioanal. Chem.*, vol. 412, no. 28, pp. 7739–7755, 2020, doi: 10.1007/s00216-020-02927-8.

[39] W. Wang, Q.-Q. Wei, J. Wang, B.-C. Wang, S. Zhang, and Z. Yuan, "Role of thiol-containing polyethylene glycol (thiol-PEG) in the modification process of gold nanoparticles (AuNPs): Stabilizer or coagulant?," *J. Colloid Interface Sci.*, vol. 404, pp. 223–229, 2013, doi: https://doi.org/10.1016/j.jcis.2013.04.020.

[40] G. S. Perera, S. A. Athukorale, F. Perez, C. U. Pittman, and D. Zhang, "Facile displacement of citrate residues from gold nanoparticle surfaces," *J. Colloid Interface Sci.*, vol. 511, pp. 335–343, 2018, doi: https://doi.org/10.1016/j.jcis.2017.10.014.

[41] X. Xia *et al.*, "Quantifying the Coverage Density of Poly(ethylene glycol) Chains on the Surface of Gold Nanostructures," *ACS Nano*, vol. 6, no. 1, pp. 512–522, Jan. 2012, doi: 10.1021/nn2038516.

[42] R. Calvo *et al.*, "Amplitude-Resolved Single Particle Spectrophotometry: A Robust Tool for High-Throughput Size Characterization of Plasmonic Nanoparticles," *Nanomaterials*, vol. 13, no. 17. 2023, doi: 10.3390/nano13172401.

[43] H.-W. Cheng, Z. Skeete, Q. M. Ngo, J. Luo, and C.-J. Zhong, "Harnessing the interparticle J-aggregate induced plasmonic coupling for surface-enhanced Raman scattering," *Phys. Chem. Chem. Phys.*, vol. 17, no. 43, pp. 28529–28533, 2015, doi: 10.1039/C5CP04920B.

[44] H.-W. Cheng *et al.*, "Assessing Interparticle J-Aggregation of Two Different Cyanine Dyes with Gold Nanoparticles and Their Spectroscopic Characteristics," *J. Phys. Chem. C*, vol. 119, no. 49, pp. 27786–27796, Dec. 2015, doi: 10.1021/acs.jpcc.5b09973.

[45] W. Leng and P. J. Vikesland, "MGITC facilitated formation of AuNP multimers," *Langmuir*, vol. 30, no. 28, pp. 8342–8349, 2014, doi: 10.1021/la501807n.

[46] X. Qian, S. R. Emory, and S. Nie, "Anchoring molecular chromophores to colloidal gold nanocrystals: Surface-enhanced Raman evidence for strong electronic coupling and irreversible structural locking," *J. Am. Chem. Soc.*, vol. 134, no. 4, pp. 2000–2003, 2012, doi: 10.1021/ja210992b.

[47] E. C. L. Le Ru *et al.*, "Experimental demonstration of surface selection rules for SERS on flat metallic surfaces," *Chem. Commun.*, vol. 47, no. 13, pp. 3903–3905, 2011, doi: 10.1039/c1cc10484e.

[48] K. M. R. Scher *et al.*, "Concentration and Surface Chemistry Dependent Analyte Orientation on Nanoparticle Surfaces," *J. Phys. Chem. C*, vol. 126, no. 38, pp. 16499–16513, 2022, doi: 10.1021/acs.jpcc.2c05007.

[49] I. I. S. Lim *et al.*, "Adsorption of cyanine dyes on gold nanoparticles and formation of J-aggregates in the nanoparticle assembly," *J. Phys. Chem. B*, vol. 110, no. 13, pp. 6673–6682, 2006, doi: 10.1021/jp057584h.

[50] N. J. Hestand and F. C. Spano, "Molecular Aggregate Photophysics beyond the Kasha Model: Novel Design Principles for Organic Materials," *Acc. Chem. Res.*, vol. 50, no. 2, pp. 341–350, Feb. 2017, doi:

Verdin, A., Malherbe, C., Sloan-Dennison, S., Faulds, K., Graham, D., & Eppe, G. (2024). Thiol-polyethylene glycol-folic acid (HS-PEG-FA) induced aggregation of Au@Ag nanoparticles: a SERS and extinction UV–Vis spectroscopy combined study. *Spectrochimica Acta - Part A: Molecular and Biomolecular Spectroscopy*, *322*, Article 124848. Advance online publication. https://doi.org/10.1016/j.saa.2024.124848

10.1021/acs.accounts.6b00576.

[51] E. Alloa, V. Grande, R. Dilmurat, D. Beljonne, F. Würthner, and S. C. Hayes, "Resonance Raman study of the J-type aggregation process of a water soluble perylene bisimide," *Phys. Chem. Chem. Phys.*, vol. 21, no. 33, pp. 18300–18309, 2019, doi: 10.1039/c9cp01874c.

[52] I. J. Jahn, A. Mühlig, and D. Cialla-May, "Application of molecular SERS nanosensors: where we stand and where we are headed towards?," *Anal. Bioanal. Chem.*, vol. 412, no. 24, pp. 5999–6007, 2020, doi: 10.1007/s00216-020-02779-2.

[53] T. Tan *et al.*, "LSPR-dependent SERS performance of silver nanoplates with highly stable and broad tunable LSPRs prepared through an improved seed-mediated strategy," *Phys. Chem. Chem. Phys.*, vol. 15, no. 48, pp. 21034–21042, 2013, doi: 10.1039/C3CP52236A.